Drivers of Spatial Variability of Subsurface Storage in the H.J. Andrews Experimental Forest

_____

Emily Crampe
CE 513: GIS in Water Resources
3/17/2019 - - Term Project Report

Webpage address: http://web.engr.oregonstate.edu/~crampee/

Introduction
Catchment subsurface storage provides water to streams during periods of low precipitation and creates a time-lagged buffer that absorbs and reduces storm-induced runoff. Quantifying the total storage of an aquifer continues to remain a challenge, but significant progress has taken place to assess fluctuations in mobile and dynamic storage (McGuire and McDonnell, 2006; Staudinger et al., 2017). Mobile storage is the water within an aquifer that can move between pore spaces in the substrate. Dynamic storage includes the water that directly influences stream processes (including water involved in evapotranspiration) (Staudinger et al., 2017). While the influence of storage is recognized, the temporal and spatial dynamics that drive its variability are not well understood. The variables that affect subsurface storage can be separated into two categories: inherit and external characteristics (Heidbüchel et al., 2013). The inherit variables are the physical attributes of the catchment, such as curvature, soil type and depth, surface roughness, and forest age and composition. The external variables include variations in the inputs to the system, such as precipitation intensity, duration, and type. The overall goal of this research is to examine groundwater storage dynamics in several small, temperate watersheds. We expect that the temporal variability of storage will relate climatic changes, while the spatial variability of storage will relate to the physical attributes of the catchments. GIS based analysis may help to determine what combinations of physical attributes determine the relative volume of subsurface storage from catchment to catchment.

In addition to the spatial data, we turn our attention to the long-term 25-year record of hydrometric and meteorological records and provide an estimate of dynamic storage using a water balance approach (Sayama et al., 2011). We acknowledge that the evapotranspiration estimates have limited accuracy, so we also examine water partitioning by isolating the two unknowns (storage and evapotranspiration) and examine changes in runoff coefficient (area weighted total annual discharge/ total annual precipitation) across the landscape and through time as a metric to track variability in water partitioning. Each watershed has a unique total average storage and average annual runoff coefficient.

Using these two approaches (spatial analysis and examining the hydrometric record) we attempt to learn more about groundwater storage dynamics through time and space. This project seeks to address the role of the spatial, inherent characteristics in driving the variability in groundwater storage we see in several temperature catchments over an averaged 25 year record.

Objective
This study incorporates several spatial datasets to understand storage dynamics at the catchment scale, with the ultimate goal of assessing the vulnerability of groundwater storage to climatic induced changes (external characteristics, i.e. changes in type, intensity, and timing of precipitation), and the role of inherit characteristics (i.e., timber harvesting, slope, and surface roughness) in minimizing that vulnerability. Several spatial analyses will be performed and used to calculate the integrative moisture index of the small watersheds in the H.J. Andrews Experimental Forest. The integrative

moisture index has primarily been used to understand potential available soil water for plants. This index has successfully been related to forest compositions, as different forest types require more or less water (Peters et al., 2010; Iverson et al., 2004; Iverson et al., 1997). The index is a function of the aspect, flow accumulation, curvature, and available water capacity of the soil columns. This project uses this same index in a new setting to determine if similar variables are driving soil moisture storage in the Western Cascades.

Site Description
The H.J. Andrews Experimental Forest (HJA) is located in the Western Cascades in Central Oregon, close to the town of Blue River (Fig. 1). The Cascades produce a rain shadow effect in this area, and because of this, HJA experiences large amounts of seasonal rainfall, averaging around 220 cm a year. The precipitation has a significant seasonal pattern with the majority of the precipitation occurring between October and April during long-duration, low intensity frontal storms (Swanson and Jones, 2002), and extremely sparse precipitation occurring in the summer months. The high elevations of HJA (>800m) develop seasonal snowpacks that can persist from November to late April (CenMet) or June (VanMet, UplMet) (Swanson and Jones, 2002; Harr and McCorison, 1979; Perkins and Jones, 2008). HJA incorporates several snow transition zones, leading watersheds to be located in the transient (WS 09, WS 10), transient to seasonal (WS 01, WS 02, WS 03) to seasonal (WS 06, WS 07, WS 08) snow zones within the Lookout Creek and Blue River basins (Jones and Perkins, 2010).

The geology of HJA is predominately igneous (Fig. 2) with formation positions largely following elevation lines. Areas lower than 760m are underlain with hydrothermally altered volcanoclastic rocks Oligocene to early Miocene in age (Little Butte Formation: massive, reddish and buff-colored tuffs and breccias derived from mudflows and pyroclastic flows). The middle to late Miocene Sardine Formation occurs between 760-1200m and consists of two units: The lower unit is similar to the underlying Little Butte, except less altered, consisting of greenish tuffs and breccias and welded and non-welded ash flows. The higher elevation unit is andesitic lava flows (Swanson and James, 1975). The Pilocascade Formation, is composed of Pliocene aged basaltic and andesitic lava flows. The southeastern portion of the forest, much of which incorporates the Mack Watershed, is riddled with glacial landforms (cirques and U-shaped valleys) and glacial till is exposed at the surface (Swanson and Jones, 2002). Steep valley walls now frequently experience debris slides. Several areas throughout the forest are subjected to deep-seated (>5m thickness) and slow moving (generally <1m/yr) earthflows resulting in irregular terrain with slopes of 5-10° (Fig. 3) (Swanson and Swanston, 1977; Pyles et al., 1987).

Data presented in this study were collected from several watersheds within HJA: Watersheds 02, 03, 07, 08, Mack, and Lookout (Fig. 4). The watersheds differ in physical attributes and have experienced different forest management applications.
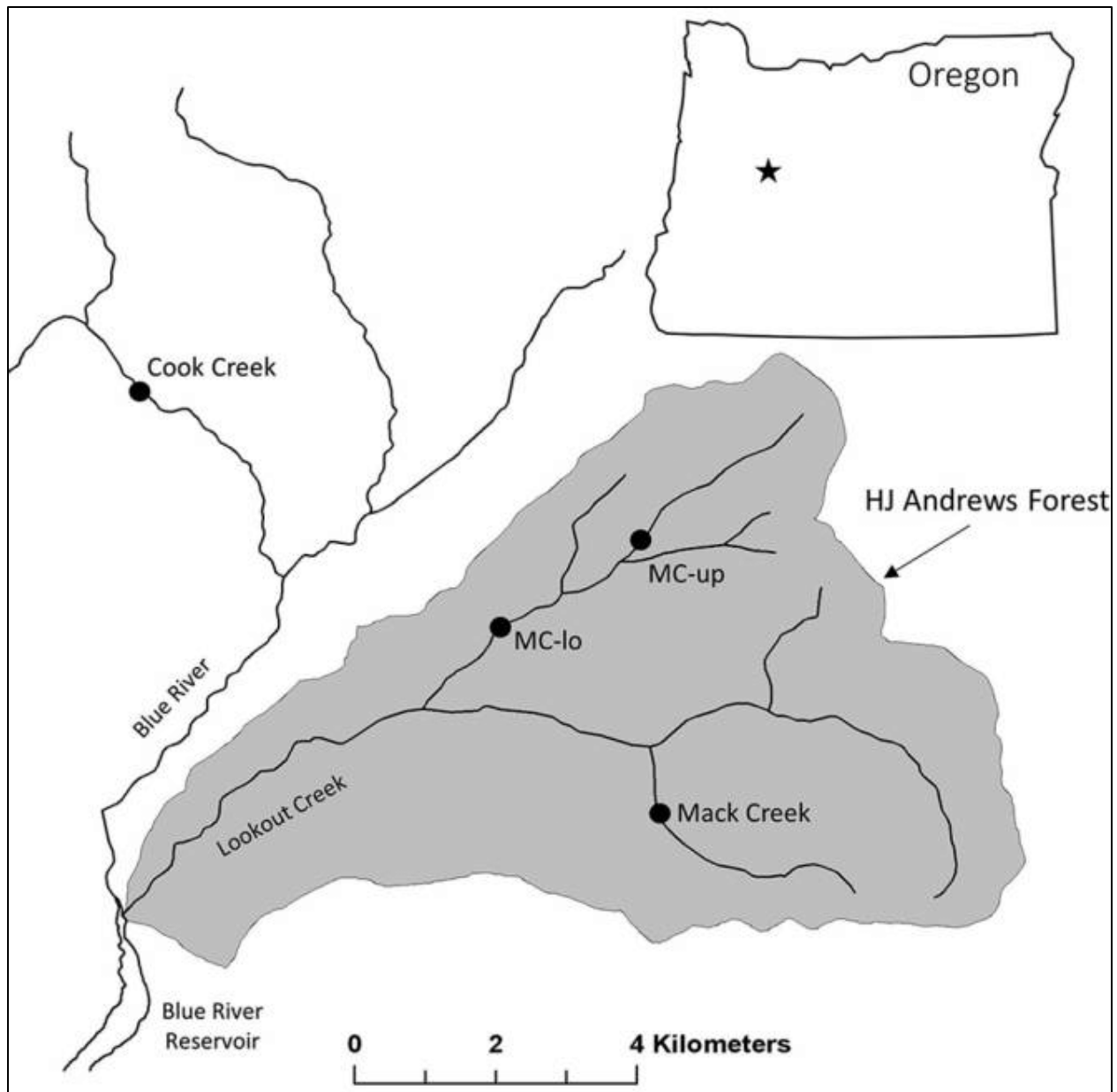
Figure 1: Location map of the H.J. Andrews Experimental Forest. Figure from Heaston et al., 2017.
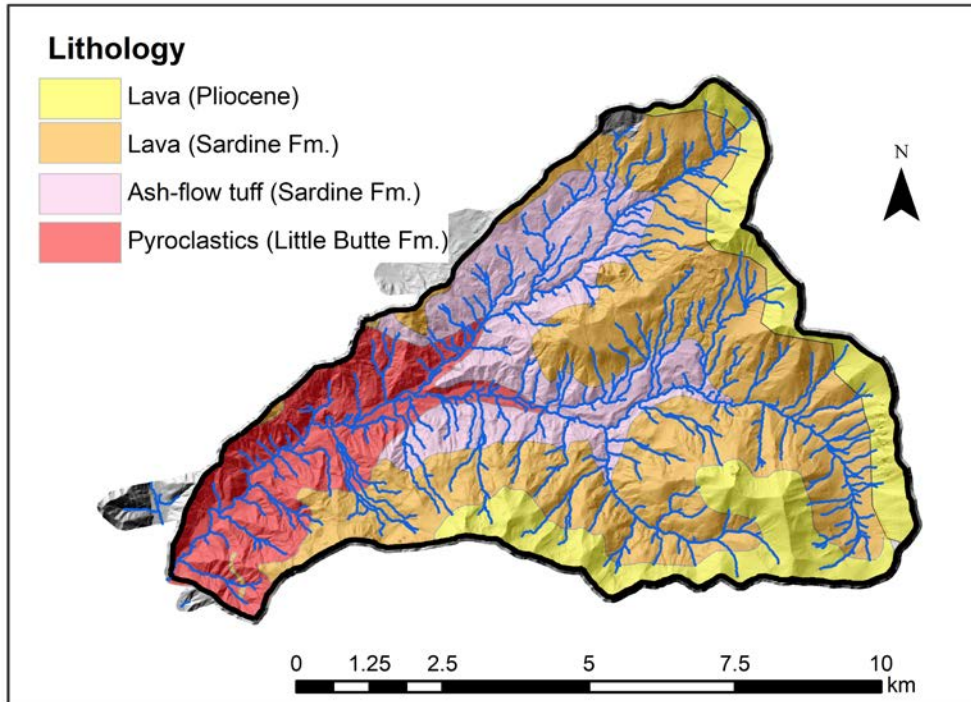
Figure 2: Geological map of the H.J. Andrews Experimental Forest.
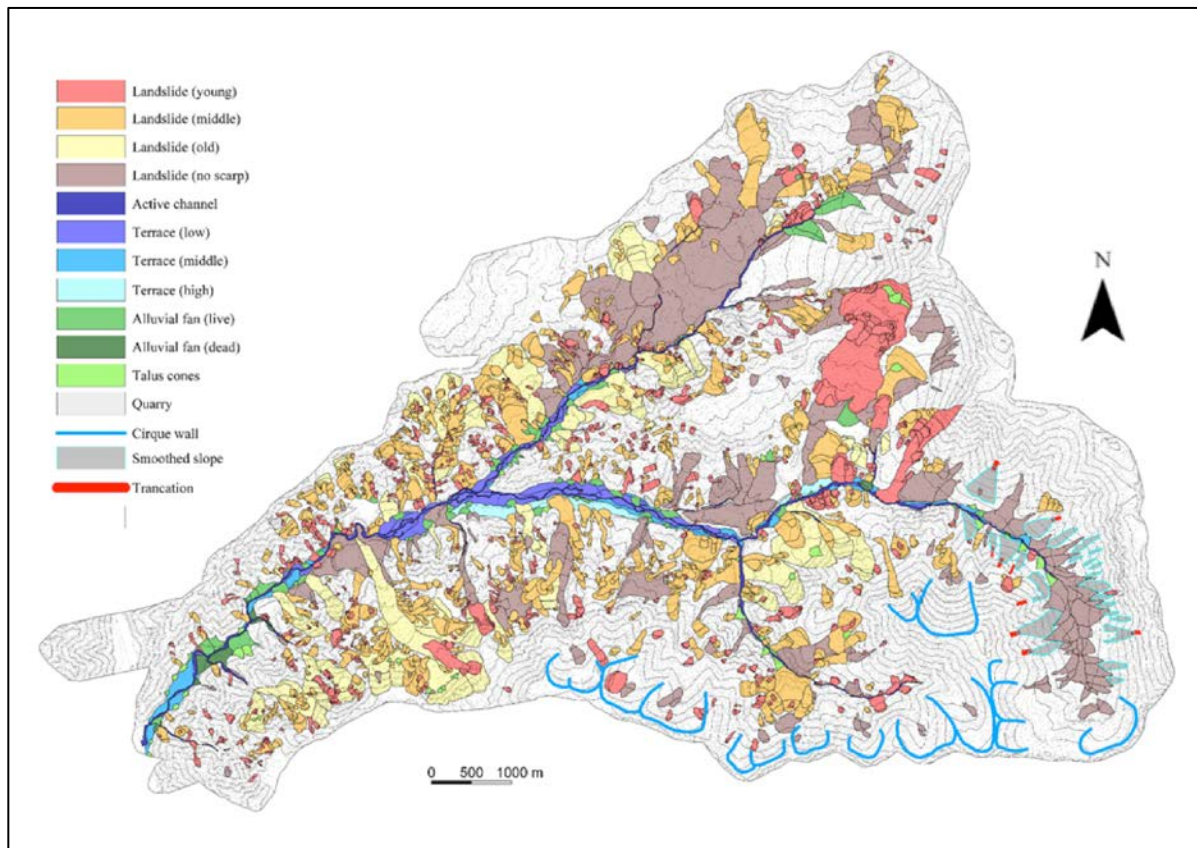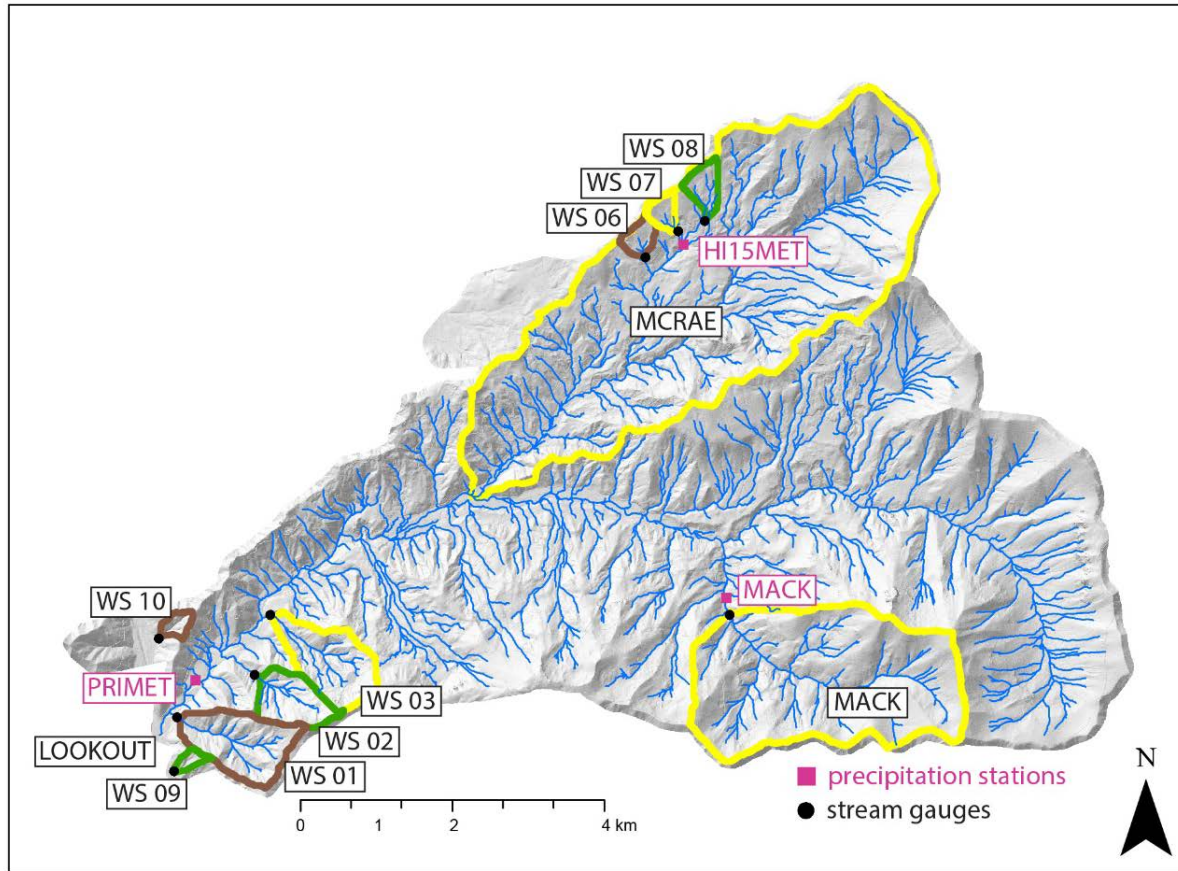

Figure 3: Slope stability map.

Figure 4: Watershed location map. Watersheds are colored by their forest management history where brown indicates a past clearcut, yellow indicates patch cuts, and green indicates that it is a reference, old growth area.

Data Description
To separate out the influence of climate and the influence of physical attributes, data were used from the small catchments throughout HJA (Fig. 4), as these catchments are variable in physical attributes (forest management history, slope, lithology, and area) but experience similar climatic inputs.

Datasets included:
1. 1m resolution Lidar derived DEM (Raster. Datum: NAD 1983)
2. Gauged watershed boundaries shapefile (Vector. Datum: NAD 1983)
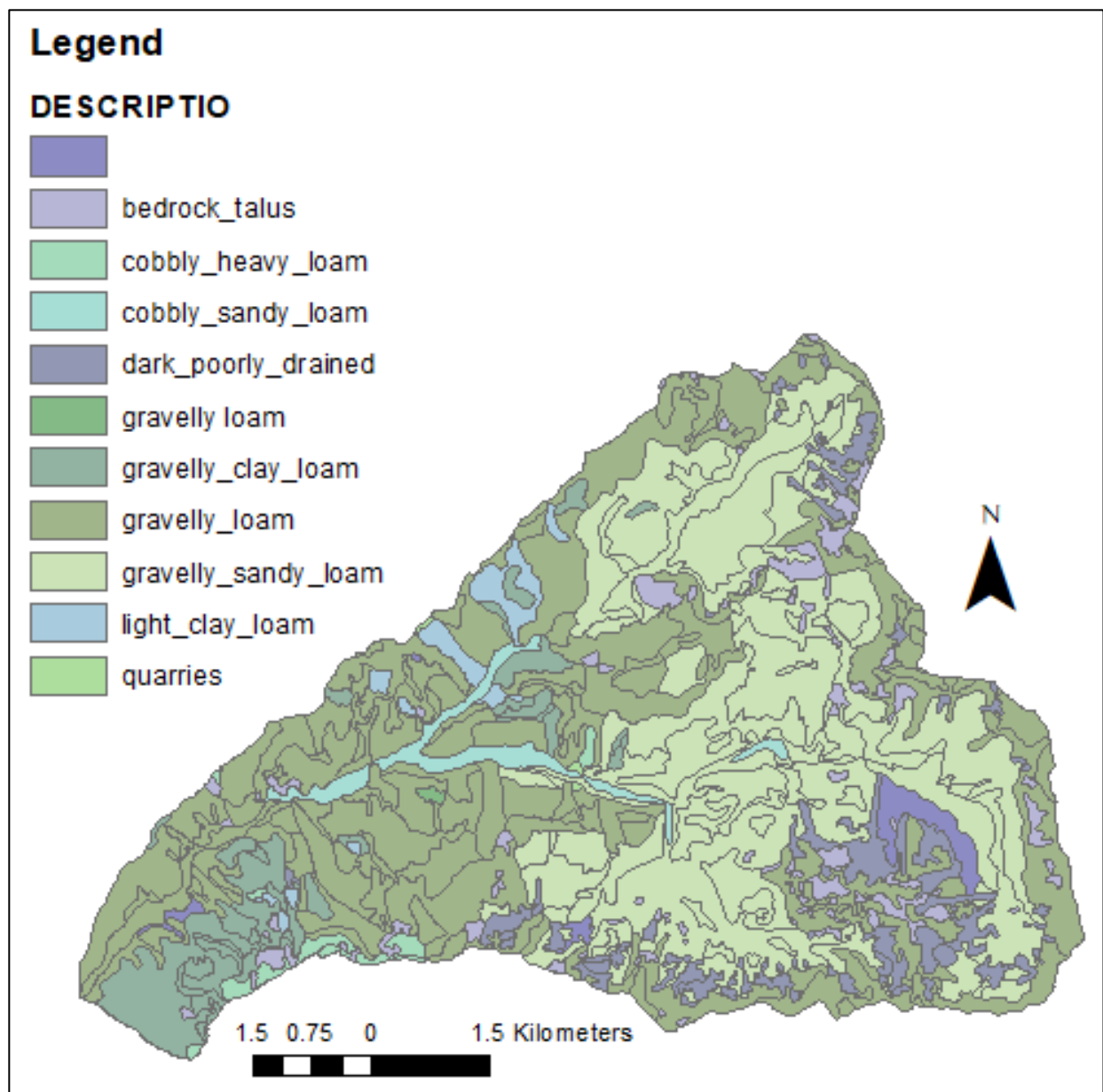3. Soil survey shapefile (Fig. 5) (Vector. Datum: NAD 1983)

Legend

DESCRIPTIO

- (no label)
- bedrock_talus
- cobbly_heavy_loam
- cobbly_sandy_loam
- dark_poorly_drained
- gravelly loam
- gravelly_clay_loam
- gravelly_loam
- gravelly_sandy_loam
- light_clay_loam
- quarries

1.5 0.75 0   1.5 Kilometers

Figure 5: Soil survey shapefile data.

Methodology

Integrated Moisture Index

Much of the methodology associated with determining the integrated moisture index (IMI) focused on creating raster files from the digital elevation model, and then manipulating these rasters so that we could weight them appropriately when calculating the index. All of the methodology steps are outlined graphically (Fig. 6) and explained in more detail below.
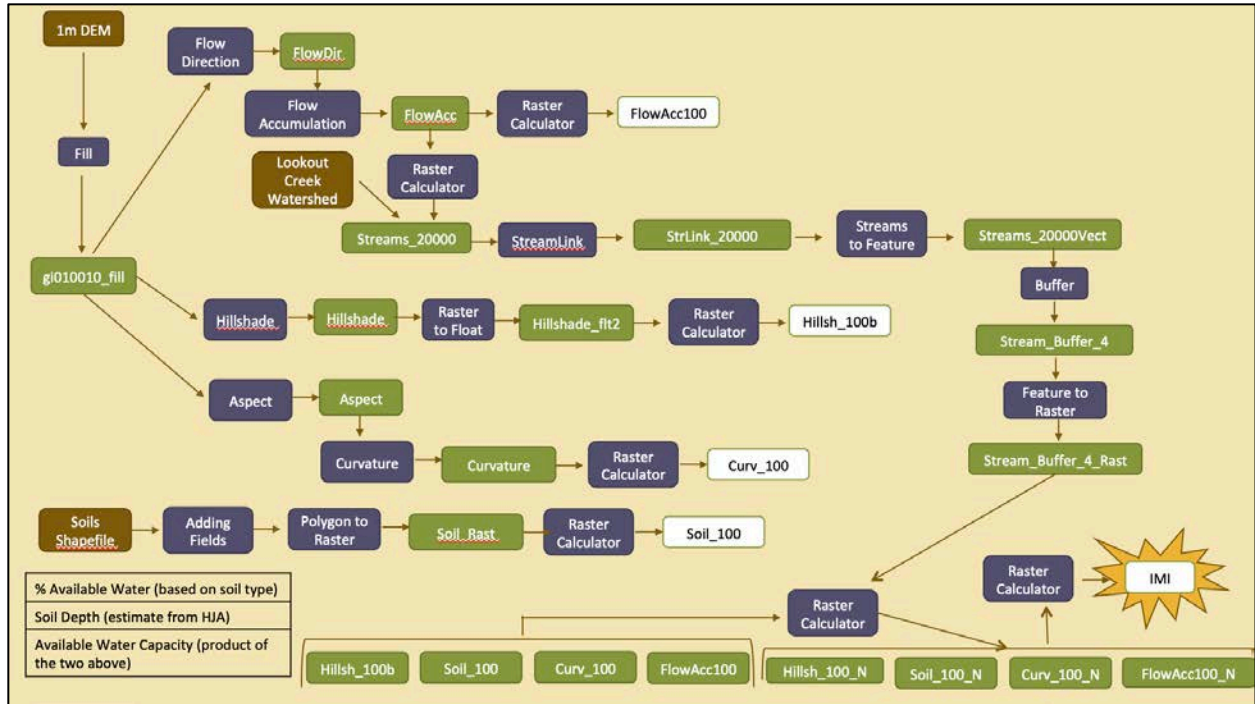
Figure 6: Graphical representation of the necessary steps to calculate the integrated soil moisture index.

1. Fill the Lidar derived 1m grid cell digital elevation model (gi010010_fill)
2. Produce flow direction raster (FlowDir) from the filled DEM (gi010010_fill)
3. Produce flow accumulation raster (FlowAcc) from the flow direction raster (FlowDir)
4. Standardize the output of the flow accumulation raster (FlowAcc) from 0 to 100 using the raster calculator (Fig. 7)
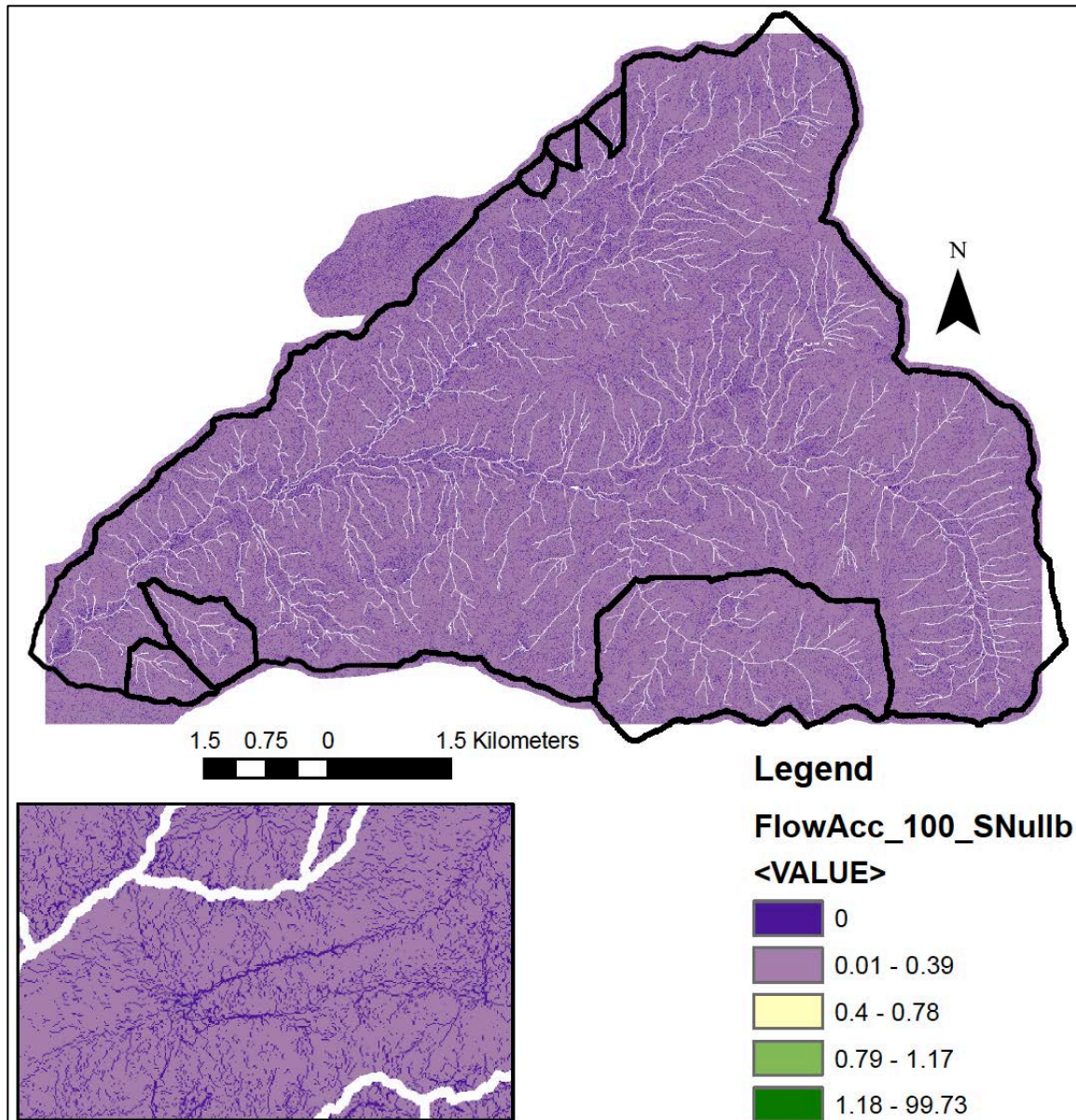
Figure 7: Standardized flow accumulation raster.

5. Define streams (Streams) from the flow accumulation raster (FlowAcc) using the raster calculator (here a stream threshold of 20,000 was assigned)
6. Produce hillshade raster (Hillshade) from the filled DEM (gi010010_fill) using the spatial analyst toolbox and, using the raster to float tool, ensure all values are floats
7. Standardize the output of the hillshade raster (Hillshade) from 0 to 100 using the raster calculator (Fig. 8)
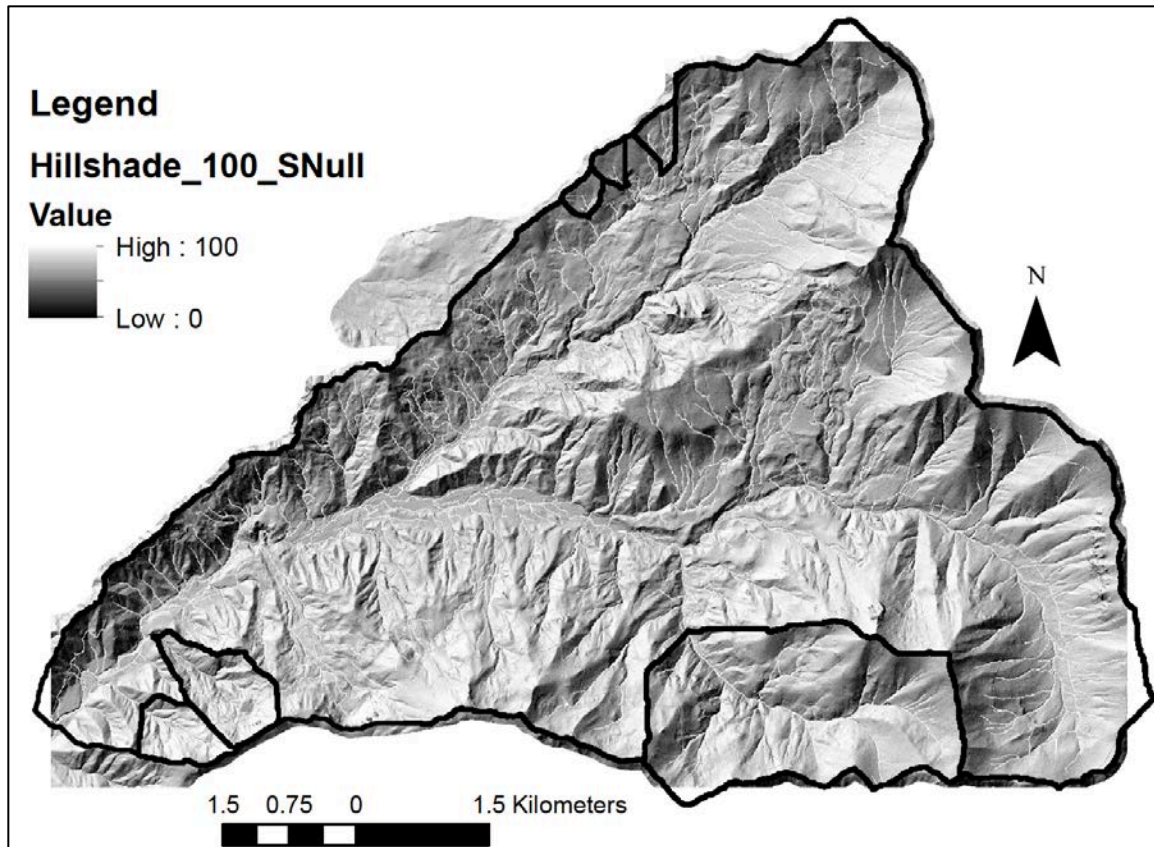
Figure 8: Standardized hillshade raster.

8. Produce aspect raster (Aspect) from the filled DEM (gi010010_fill)
9. Calculate curvature (Curvature) from the aspect raster (Aspect)
10. Standardize the output of the curvature raster (Curvature) from 0 to 100 using the raster calculator (Fig. 9)
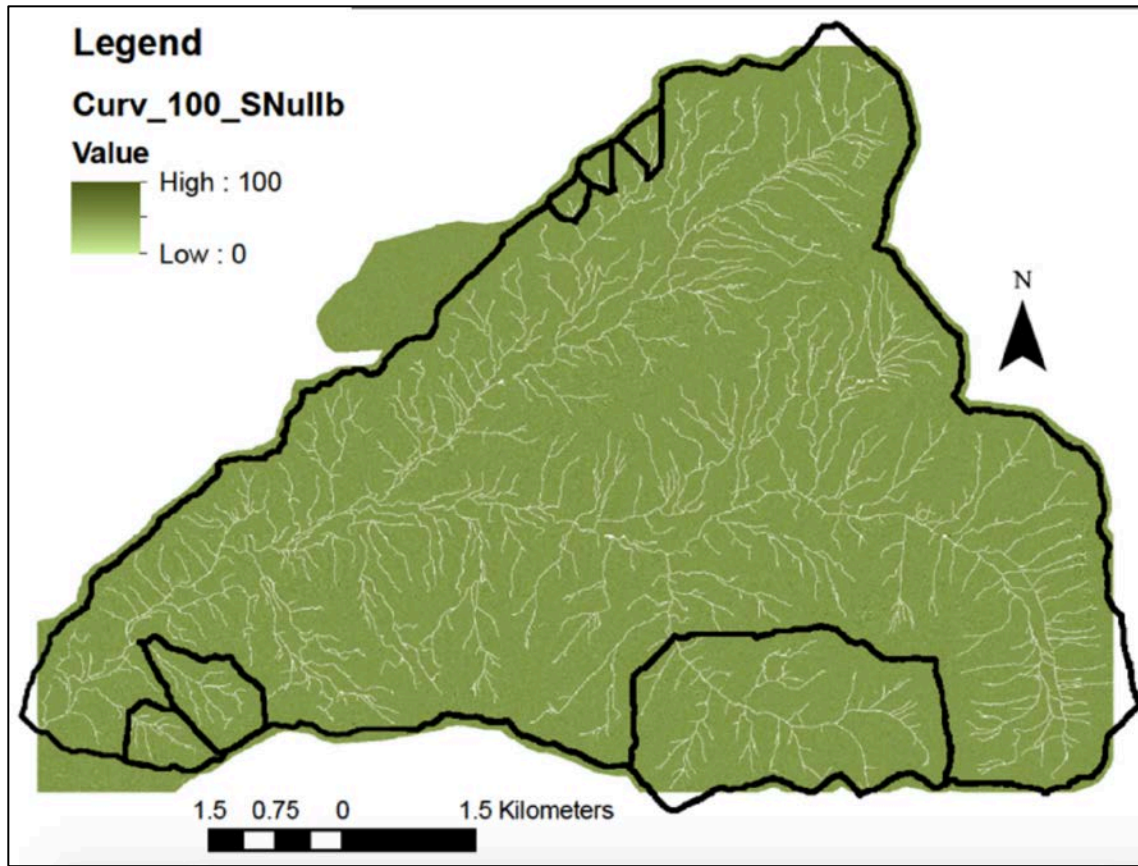
Figure 9: Standardized curvature raster.

11. Using the soil vector shapefile, calculate the percent plant available water (field capacity – wilting point) for each soil textural class using lab derived estimates (Table 1)

Table 1: Lab derived estimates of percent available water for common soil textural classes. Table from Easton and Bock, 2016.

Textural class	Wilting point	Field capacity	Available water
	(% moisture)		
Sand	5	12	7
Sandy loam	9	21	12
Loam	16	36	20
Silt loam	18	39	21
Clay loam	24	39	15
Silty clay	24	39	13
Clay	27	39	12

12. Calculate the average soil depth for each polygon
13. Calculated available water capacity by multiplying the percent plant available water by the depth of the soil
14. Using the polygon to raster tool, convert the vector available water capacity (SoilWCapVect) to a raster (SoilWCapRast)
15. Standardize the output of the soil raster (SoilWCapRast) from 0 to 100 using the raster calculator (Fig. 10)
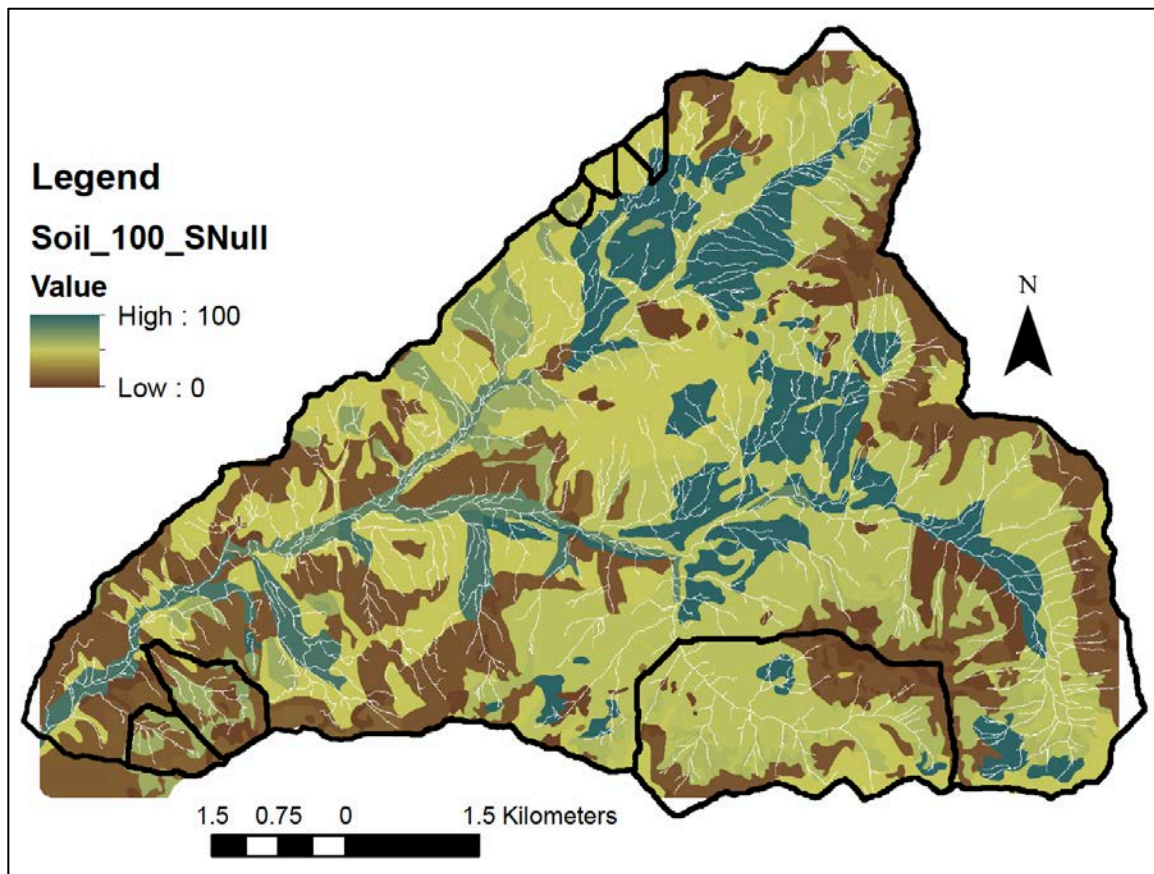

Figure 10: Standardized available water capacity raster.

16. Create stream links using the delineated stream network (Streams) and convert this layer to a vector using the Streams to Feature function
17. Create a buffer of 4 meters around the vector stream network (Stream_Vect) to focus on soil moisture estimation for the hillslopes rather than areas that are saturated or within the hyporheic zone
18. Make the vector buffered area into a raster using the Feature to Raster tool
19. Delete buffered area from all rasters (Hillshade, Curvature, FlowAcc, SoilWCapRast), creating (HillshadeB, CurvatureB, FlowAccB, SoilWCapRastB) using the Set_Null expression in the raster calculator
20. Calculate the Integrate Moisture Index (IMI) using the Raster Calculator

IMI = [Hillshade * 0.4] + [Curvature(ϴ) * 0.1] + [FlowAcc * 0.3] + [SoilWCapRast * 0.2]

The resulting index will vary between 0 and 100, with 100 being areas with the largest amount of moisture, and therefore the highest soil moisture storage (Fig. 11)
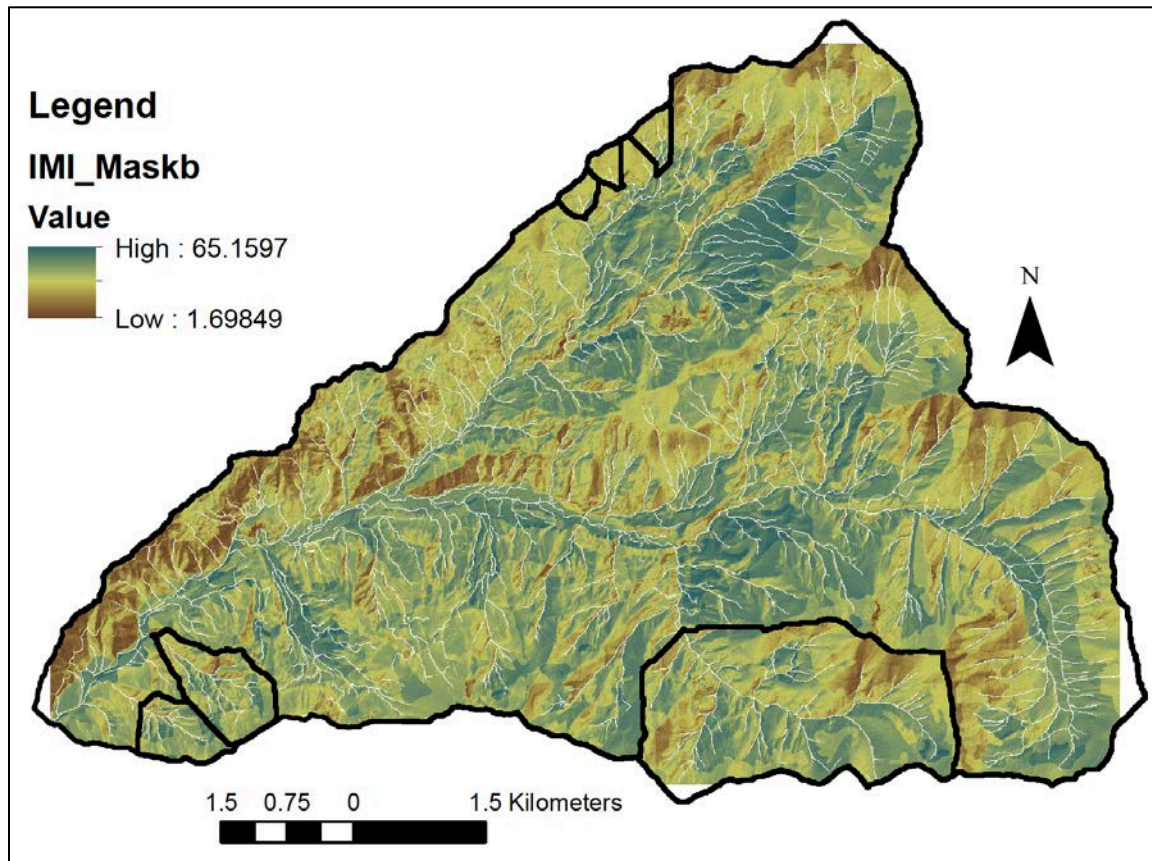

Figure 11: Standardized integrated moisture index raster.

21. Using zonal statistics determine the mean IMI for each of the small watersheds using the gauged watershed boundary shapefile (wsheddem)

Water Balance and Runoff Coefficients
Using the 25 year long hydrometric record, two more metrics were calculated to compare to the IMI to assess the accuracy of this tool. Using the water balance approach (Sayama et al., 2011) where:

Changes in Storage = Precipitation – Area Weighted Discharge – Evapotranspiration

estimates of groundwater storage were calculated for Watersheds 02, 03, 06, 07, 08, and Mack. Evapotranspiration was estimated using the Hamon method, a temperature based evaluation. Because plants in this region are water limited in the summer, rather than radiation or temperature limited, the Hamon method may over estimate evapotranspiration. To avoid this issue, a second metric, annual average runoff

coefficient, was also calculated. For this analysis, our two unknowns of evapotranspiration and storage are lumped together.

Annual Average Runoff Coefficient = Total Annual Area Weighted Discharge/ Total Annual Precipitation

This metric assesses water partitioning on the catchment scale, as we are able to see what percentage of the input is sectioned off to discharge.

Results
In order to summarize the results, the IMI values were average across the small watersheds using zonal statistics. The standalone IMI values do not provide us with much information, but when the values are compared between watersheds we are able to see which watersheds have more potential for soil moisture storage. IMI values are lowest for Watersheds 06, 07, and 08, while Watersheds 02, 03, and Mack have higher potentials (Fig. 11; Table 2).

Watersheds 06 and Mack have the lowest average annual storage, while Watersheds 08 and 07 have the highest (Table 2). The lowest annual average runoff coefficients are observed in Watersheds 07 and 03, while Watersheds 06 and Mack have the highest (Table 2). These results follow the expected trend, as watersheds with high annual storage have low runoff coefficients (Fig. 12). Any deviations from this trend are due to the evapotranspiration estimates. However, the water balanced based storage values and the average annual runoff coefficient values do not follow the trend that is observed in the IMI values, meaning watersheds with high annual storage and low runoff coefficients do not necessarily have the highest IMI values (Fig. 13; Fig 14).

Table 2: Summary of the three metrics used to evaluated mobile, dynamic storage

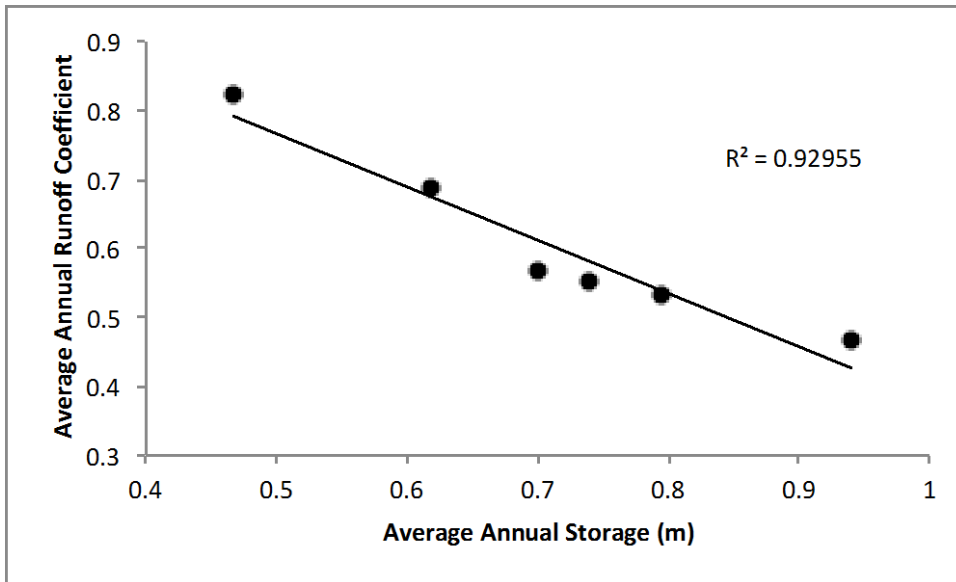| Watershed	Average IMI Value	Avg Annual Storage (m)	Avg Annual Runoff Coefficient
WS 07	35.4972371	0.94	0.467
WS 06	37.56870545	0.618	0.687
WS 08	38.72967958	0.795	0.533
MACK	40.91615665	0.467	0.821
WS 03	42.06902791	0.739	0.55
WS 02	44.4861325	0.701	0.565

Figure 12: Comparison of the average annual storage and average annual runoff coefficient metrics. There is a significant relationship between the two, with deviations from this relationship arising from inaccurate evapotranspiration calculations.
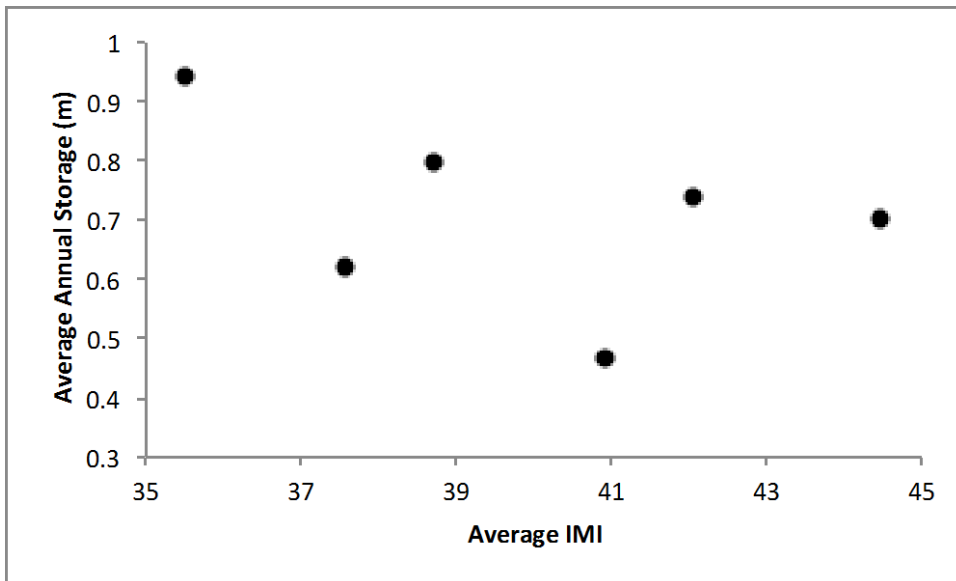

Figure 13: Comparison of the average annual storage and IMI metrics. There is no significant relationship.
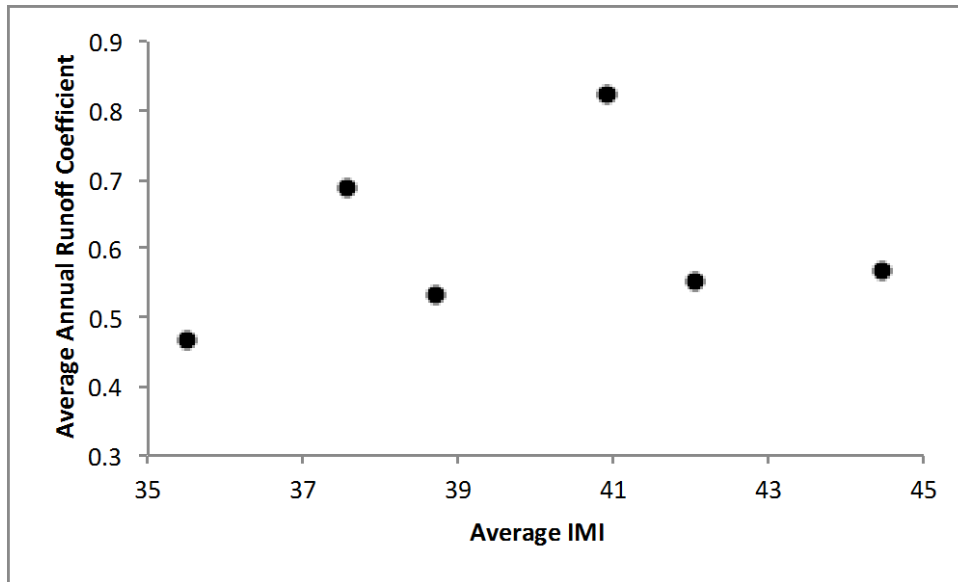
Figure 14: Comparison of the average annual runoff coefficient and IMI metrics. There is no significant relationship.

Discussion and Conclusions

The IMI did not replicate relative subsurface storage results that were determined through other metrics. Previously, the IMI has been used predominately in Ohio to determine forest composition (Peters et al., 2010; Iverson et al., 2004; Iverson et al., 1997). This project suggests that the IMI in its current form is not applicable at the catchment scale in the Western Cascades. It is possible that with some adjustments (changing the weighting factors or adding a variable for surface roughness), the IMI could be a tool to understand the dynamic, mobile storage variability caused by the physical attributes of these catchments.

References

Easton, Z.M. and Bock, E. 2016. Soil and Soil Water Relationships. Virginia
    Cooperative Extension. BSE 194P.

Harr, R.D., and McCorison, F.M. 1979. Initial effects of clearcut logging on size and
    timing of peak flows in a small watershed in western Oregon. Water Resources
    Research. 15 (1): 90-94.

Heaston, E.D., Kaylor, M., and Warren, D. 2017. Characterizing short-term light
    dynamics in forested headwater streams. Freshwater Science. 36(2):000-000.

Heidbüchel, I., Troch, P.A., and Lyon, S.W. 2013. Separating physical and
    meteorological controls of variable transit times in zero-order catchments. Water
    Resources Research. 49: 7644-7657.

Iverson, L.R., Prasad, A.M. and Rebbeck, J. 2004. A comparison of the integrated
    moisture index and the topographic wetness index as related to two years of soil
    moisture monitoring in Zaleski State Forest, Ohio. Proceedings of the 14th
    Central Hardwoods Forest Conference.

Iverson, L.R., Scott, C.T., Dale, M.E., and Prasad, A. 1997. Development of an
    integrated moisture index for predicting species composition.

Jones, J.A. and Perkins, R.M. 2010. Extreme flood sensitivity to snow and forest
    harvest, western Cascades, Oregon, United States. Water Resources Research.
    46 W12512

McGuire, K.J. and McDonnell, J.J. 2006. A review and evaluation of catchment transit
    time modeling. Journal of Hydrology. 330: 543-563.

Perkins, R.M., and Jones, J.A. 2008. Climate variability, snow, and physiographic
    controls on storm hydrographs in small forested basins, western Cascades,
    Oregon. Hydrological Processes. 22: 4949-4964.

Peters, M., Iverson, L.R., and Prasad, A.M. 2010. Using an integrated moisture index to
    assess forest composition and productivity. USDA Forest Service Publication.

Pyles, M.R., Mills, K., and Saunders, G. 1987. Mechanics and Stability of the Lookout
    Creek Earth Flow. Environmental and Engineering Geoscience. (2): 267-280.

Swanson, F.J., and James, M.E. 1975. Geology and geomorphology of the HJ Andrews
    Experimental Forest, western Cascades, Oregon. Food and Agriculture
    Organization of the United Nations.

Swanson, F.J. and Jones, J.A. 2002. Geomorphology and hydrology of the H.J.
    Andrews Experimental Forest, Blue River, Oregon. Field Guide to Geologic

Processes in Cascadia: Oregon Department of Geology and Mineral Industries Special Paper 36.

Swanson, F.J. and Swanston, D.N. 1977. Complex mass-movement terrains in the western Cascade Range, Oregon. Geological Society of America: Reviews in Engineering Geology Volume III